A Study of Unsteady Aerodynamic Characteristics of an Accelerating Aerofoil

Young-Ki Lee†, Heuy-Dong Kim* and Srinivasan Raghunathan**

가속익의 비정상 공력특성에 관한 연구

이영기†· 김희동*· Srinivasan Raghunathan **

Key Words : Aerofoil(익형), Unsteady Flow(비정상유동), Accelerating Flow(가속유동), Aerodynamic Drag(공력저항), Shockwave(충격파)

Abstract

Flight bodies are subject to highly unstable and severe flow conditions during taking-off and landing periods. In this situation, the flight bodies essentially experience accelerating or decelerating flows, and the aerodynamic characteristics can be completely different from those of steady flows. In the present study, unsteady aerodynamic characteristics of an aerofoil accelerating at subsonic speeds are investigated using a computational method. Two-dimensional, unsteady, compressible Navier-Stokes simulations are conducted with a one-equation turbulence model, Spalart-Allmaras, and a fully implicit finite volume scheme. An acceleration factor is defined to specify the unsteady aerodynamics of the aerofoil. The results show that the acceleration of the subsonic aerofoil generally leads to a variation in aerodynamic characteristics and it is more significant at angles of attack.

1. Introduction

Wing aerodynamics has been one of the most classical and popular research areas due to a variety of its applications such as aircraft[1], missiles[2], helicopters[3] and turbomachinery[4]. The aerodynamic characteristics and various steady flow features have been well understood for subsonic to supersonic flight/operating conditions owing to the considerable efforts made through a number of experimental and numerical studies for many decades. Nonetheless, unsteady flow features and shock-boundary layer interaction occurring in the flowfield over aerofoils and associated phenomena such as dynamic stall[5], buffeting[6] and hysteresis behaviors[7] at high angles of attack are not fully understood yet.

In flight, flow unsteadiness is inevitably existent at any flight condition due to two different reasons, say, time-dependent disturbances or self-generated and self-sustained flow instabilities. Regarding the former reason, especially, an abrupt change in the flight speed can be an important source of external disturbances and it has been well known through past investigations[8]. The unsteadiness due to a gradual speed change at subsonic speeds, meanwhile, has not been investigated to date to the authors' knowledge even though it generally happens for most aircraft.

Flight bodies experiences gradually accelerating or decelerating flows essentially at taking-off and landing with angles of attack. Especially, when a shockwave is onset on an aerofoil, even a slight speed change can lead to a significant variation in SBLI (shock-boundary layer interaction) features, which are generically unsteady and have strong instability. Thus this type of

† 안동대학교 기계공학부
E-mail: kimhd@andong.ac.kr
TEL: (054) 820-5622 FAX: (054) 823-5495
* 안동대학교 기계공학과
** School of Aeronautical Engineering, The Queen's University of Belfast, United Kingdom

speed-up or speed-down can introduce a continuous but irregular change in the SBLI features and associated wake flow in the boundary layer separation. In this situation, it is expected that the aerodynamic characteristics of aerofoils can depend on the history of the speed change.

In this study, unsteady aerodynamic characteristics of an aerofoil, NACA0012, accelerating at subsonic speeds were numerically investigated. The present CFD (computational fluid dynamics) analysis was carried out using 2-dimensional unsteady compressible Navier-Stokes equations with the Spalart-Allmaras[9] turbulence model, discretized by a fully implicit finite volume scheme.

2. Numerical Simulations

2.1 Governing Equations

Mass averaged, two-dimensional unsteady Navier-Stokes equations governing the flowfield around a NACA0012 aerofoil are given in differential form as follows:

$$\frac{\partial r}{\partial t}+\frac{\partial}{\partial x_i}(ru_i)=0 \tag{1}$$

$$\frac{\partial}{\partial t}(ru_i)+\frac{\partial}{\partial x_j}(ru_iu_j)=\frac{\partial}{\partial x_j}m\left(\frac{\partial u_i}{\partial x_j}+\frac{\partial u_j}{\partial x_i}\right)-\frac{\partial}{\partial x_i}\left(\frac{2}{3}m\frac{\partial u_l}{\partial x_l}\right) -\frac{\partial p}{\partial x_i}+\frac{\partial}{\partial x_j}(-r\overline{u_i'u_j'}) \tag{2}$$

$$\frac{\partial}{\partial t}(rE)+\frac{\partial}{\partial x_i}(ru_iH)=\frac{\partial}{\partial x_i}\left[\left(x+\frac{m_t}{\Pr_t}\right)\frac{\partial T}{\partial x_i}+u_j(t_{ij})_{eff}\right] \tag{3}$$

The governing equations are discretized by an implicit finite volume scheme spatially and an explicit 4-stage Runge-Kutta time stepping scheme temporally.

The Spalart-Allmaras turbulence model was employed to close the governing equations. The turbulence model is a one-equation model recently developed, basically, for aerodynamic applications.[9] According to past studies[10] using this model, it can give good results not only for a prediction of adverse pressure gradients inside boundary layers but also for various unsteady problems issued in wing aerodynamics.

2.2 Grid System and Analysis

Fig. 1 shows the grid layouts of a C-typed computational domain and the near-field of the NACA0012 profile used in the present study. About 15,000 nodes were applied to the computational domain, in which grids were clustered in the regions near wing surfaces in order to provide accurate predictions of shock-induced flow separation. The computational domain were set up with dimensions of 20 times of the chord c towards upstream from the leading edge and 25 times of c towards downstream from the trailing edge to ensure free stream conditions and to obtain better convergence.

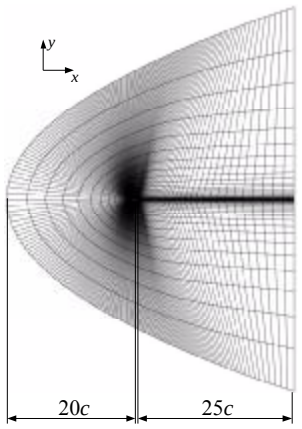

(a) Computational domain

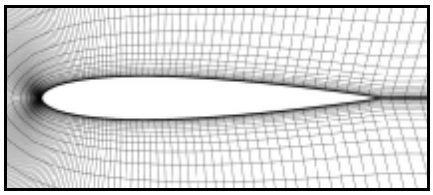

(b) Grid layout near the aerofoil model

Fig. 1 2-dimensional structured grid system for NACA0012

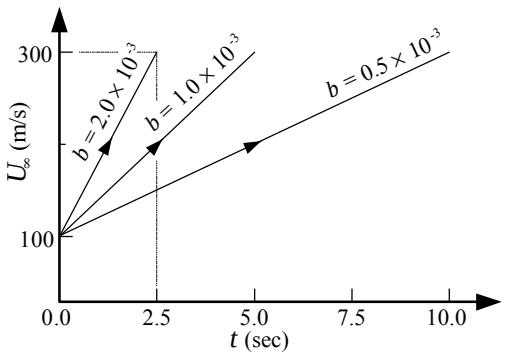

Fig. 2 Non-dimensional acceleration factor

The far-field boundary condition was applied to external boundaries of the computational domain. The free stream velocity U_∞ changes from 100 m/s to 300 m/s during the time-dependent speed-up at constant acceleration. For simplicity, a constant pressure of

101325 Pa and a constant temperature of 300 K were used for the free stream boundaries.

To give different acceleration characteristics of the aerofoil, a non-dimensional acceleration factor b was defined as follows:

$$b = \frac{(U_f - U_i)/T}{U_m / T_c} \tag{4}$$

Where, U_f, U_i and U_m are the final, initial and mean velocities respectively. T is time needed for the acceleration from U_i to U_f, and T_c is time required for a flow particle with U_m to pass through the characteristic length of the aerofoil. As shown in Fig. 2, three values of b were tested at angles of attack of 0° ~ 10°.

Unsteady solutions were initialized from a steady state solution obtained for U_∞ = 100 m/s with the criteria for both residuals of all equations (less than 1.0×10^{-4}) and drag convergence (ΔC_D, less than 1.0×10^{-7}). Time step sizes of 0.5×10^{-3} ~ 1.0×10^{-3} sec were selected in consideration of proper convergence satisfying the above criteria within 30 iterations for each time step. From the preliminary tests with several time step sizes, it has been found that a change in the drag coefficient C_D is negligible when a time step size is less than 1.0×10^{-3} sec.

3. Results and Discussion

The Mach number contours at a = 0° given in Fig.3 show the effect of accelerating time on the flowfield near the aerofoil model. The figures were selected for several representative conditions including strong shock-boundary layer interaction. As the aerofoil accelerates, typically, local supersonic regions increase and a shockwave suddenly occurs near the maximum thickness of the aerofoil. The shock moves rapidly towards the trailing edge with further increases in U_∞ and, consequently, the boundary layer behind the shock is separated (U_∞ = 300 m/s) by strong adverse pressure gradients there. With larger b, the generation of the shock and its rearward movement are retarded. At b = 2.0×10^{-3} and U_∞ = 300 m/s, shock-induced separation is apparently weak when compared with the steady state (b = 0).

Fig. 4 shows surface pressure distributions, given as the pressure coefficient C_p, with time for b = 0.5×10^{-3}, 1.0×10^{-3} and 2.0×10^{-3} (corresponding acceleration a = 20 m/s^2, 40 m/s^2 and 80 m/s^2 respectively). The pressure coefficients given in the figures are only presented for the suction side because the NACA0012 profile is exactly symmetric, resulting in basically same distributions on both sides. Surface pressure decreases from the leading edge up to about 14 % chord (the maximum thickness is at about 30 % chord) and then increases along the curved surface with a thickened boundary layer. As long as the entire flowfield is subsonic, the location of the minimum pressure is nearly fixed at about x/c = 0.14. When a local supersonic region occurs at high subsonic speeds after 0.8 U_f, however, local acceleration along the curved surface is continued up to the presence of a sudden rise in pressure due to a shockwave. For all b, a similar trend of time-dependent C_p distributions is observed but shock generation and movement are shown to be relatively abrupt at lower b.

Fig. 5 shows the Mach number contours obtained for b = 0, 1.0×10^{-3} and 2.0×10^{-3} at an angle of attack of 10°. At the given a, a local supersonic flow with a shockwave occurs considerably earlier compared with the cases at zero angle of attack. It is observed that even a weak shockwave can induce large boundary layer separation on the suction side (U_∞ = 250 m/s) and further acceleration leads to a rearward shock movement with reduced separation on the aerofoil. The effect of b on shock generation and movement is found to be similar to the cases at zero angle of attack but more noticeable particularly at a high speed of 300 m/s.

At b = 0.5×10^{-3}, the pressure distributions shown in Fig. 6 present the influence of angle of attack on accelerating flow over the aerofoil. For a low angle of attack of 2°, the change in local C_p values with time shows similar aerodynamic characteristics to the values at a = 0° on both sides. At relatively high angles of attack, 5° and 10°, C_p distributions show opposite profiles between both sides without a shockwave while follow the similar chordwise variations as those at zero angle of attack with a shockwave. It is interesting to note that the minimum C_p value and maximum shock strength are observed when the shock begins to occur. At higher angles of attack, as the shock is generated earlier, the shock on the suction side reaches its maximum strength more quickly. Then the shock becomes weaker with rearward movements during further acceleration.

Fig. 7 shows time-dependent drag histories given by C_D values for b = 0.5×10^{-3}, 1.0×10^{-3} and 2.0×10^{-3} at zero angle of attack. The C_L variations for NACA0012 at zero angle of attack are insignificant due to the symmetry of the model so that a C_L history is not given in this figure. The C_L at first remains nearly constant if the entire flowfield is subsonic. Then it is fluctuating as a local supersonic region increases during acceleration and suddenly rises in the presence of a shockwave.

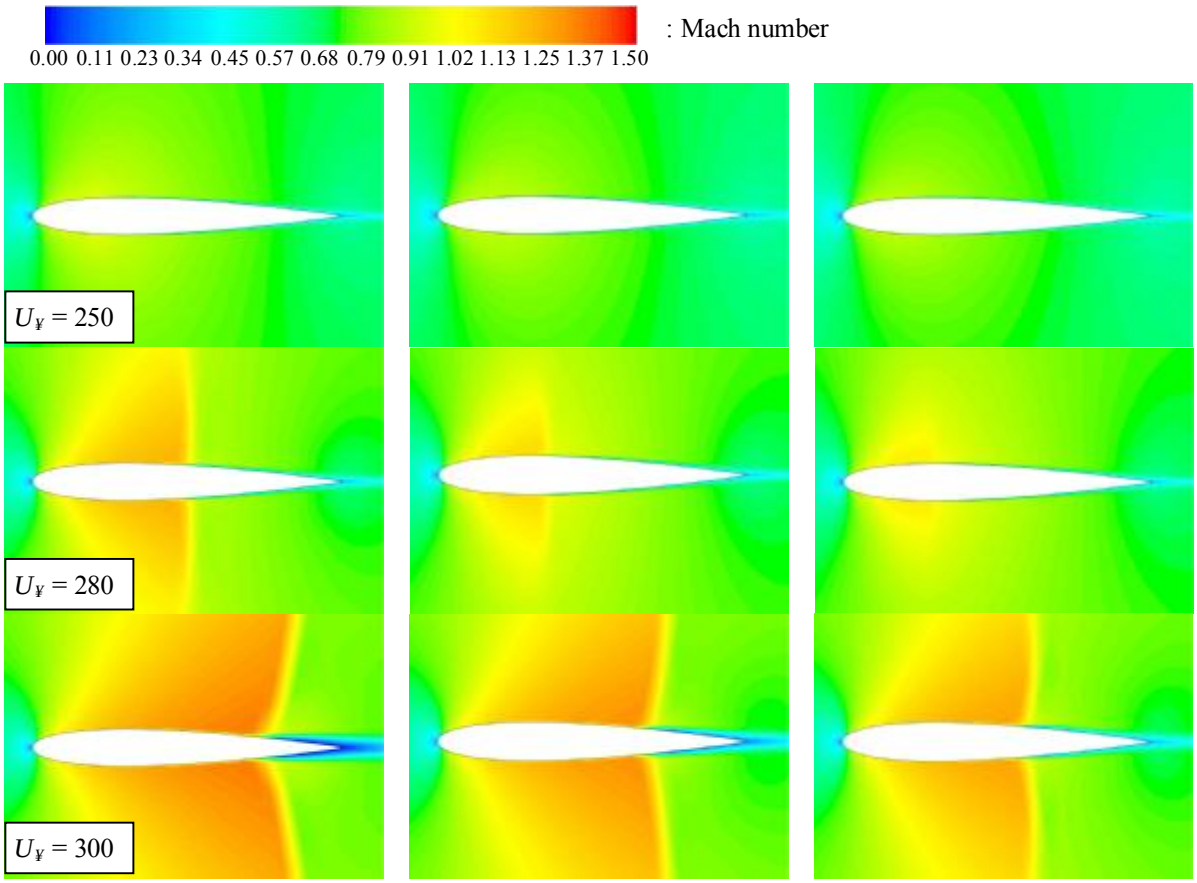

(a) $b = 0$ (steady state) (b) $b = 1.0\times10^{-3}$ (c) $b = 2.0\times10^{-3}$

Fig. 3 Mach number contours for several b at $a = 0°$

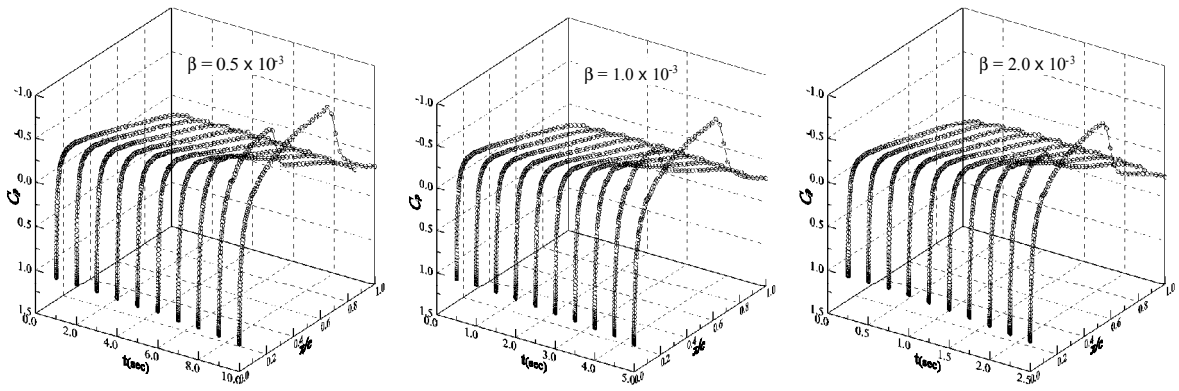

(a) $b = 0.5\times10^{-3}$ (b) $b = 1.0\times10^{-3}$ (c) $b = 2.0\times10^{-3}$

Fig. 4 Surface pressure distributions for several b at $a = 0°$

With an increase in b, C_D values become lower due to a weaker shock-boundary layer interaction at a given time step as aforementioned with the previous figures (Fig. 3 and Fig.4). Also at a high angle of attack of 10° (Fig. 8), these aerodynamic characteristics can be observed but the fluctuations are present from the beginning of acceleration. As the shockwave occurs from a low speed of about 140 m/s, a reduction of C_D is shown in a wide range of time t/T. Regarding lift (Fig. 8b), the effect of b on a time-dependent C_L variation is also significant at a low speed less than around 160 m/s. Therefore, the control of flight bodies at taking-off or at landing must be conducted in consideration of particular aerodynamic characteristics for given accelerating time and speed range.

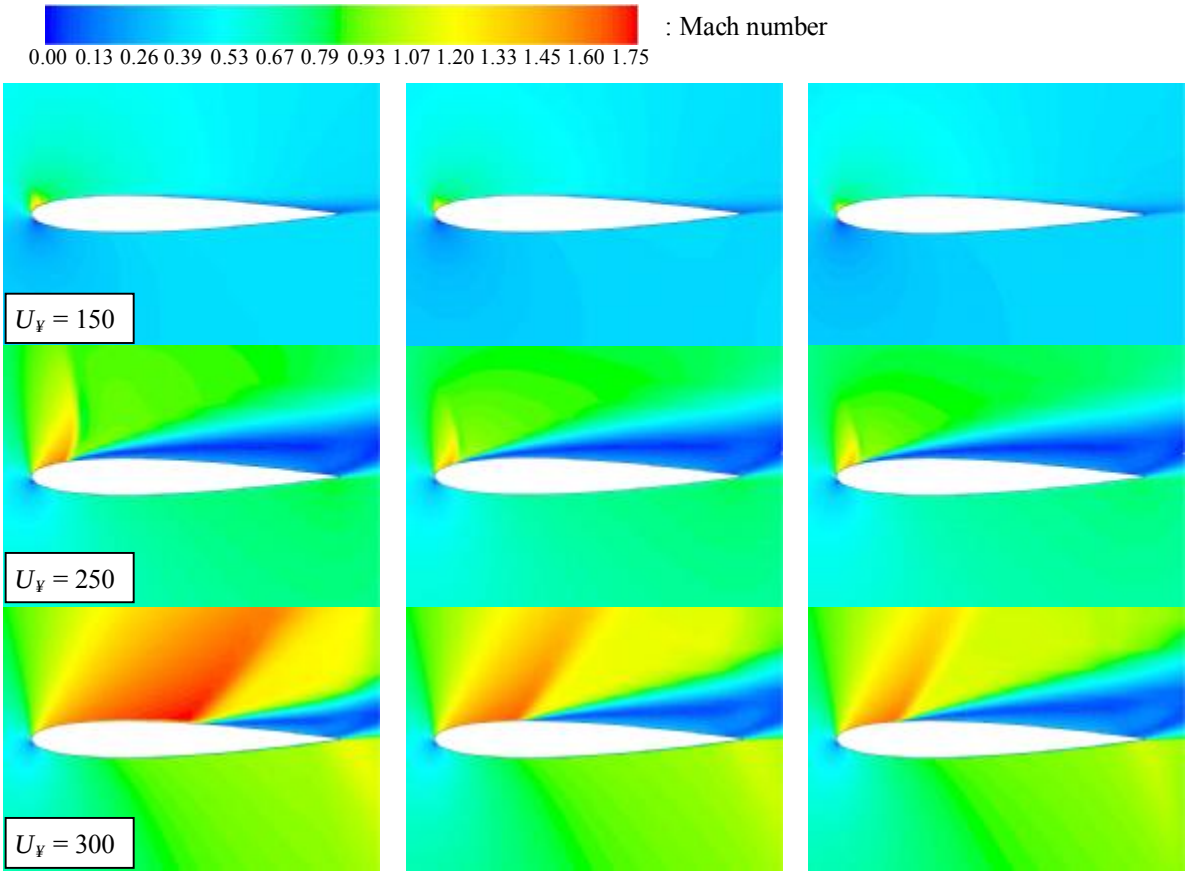

(a) b = 0 (steady state) (b) $b = 1.0\times10^{-3}$ (c) $b = 2.0\times10^{-3}$

Fig. 5 Mach number contours for several b at a = 10°

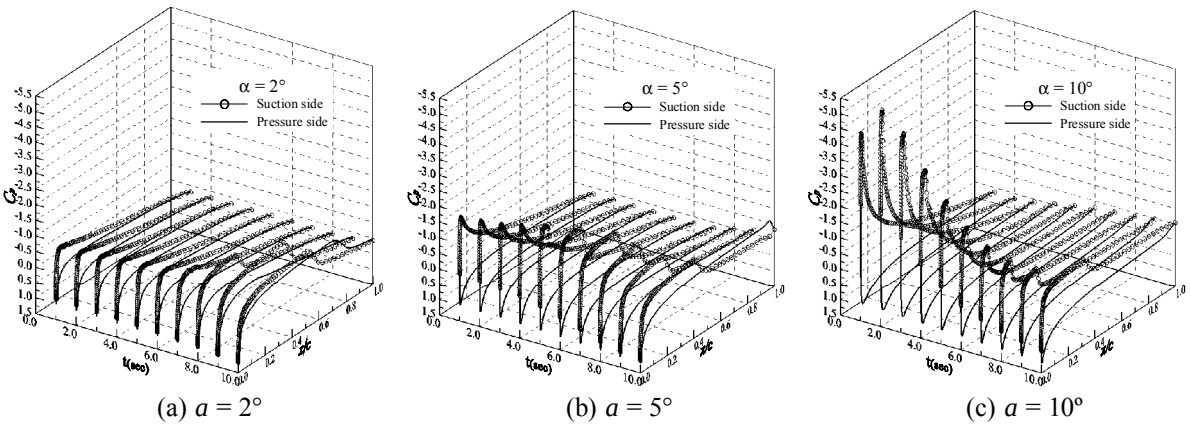

(a) a = 2° (b) a = 5° (c) a = 10°

Fig. 6 Surface pressure distributions for $b = 0.5 \times 10^{-3}$ at angles of attack

4. Conclusions

An understanding of the unsteady aerodynamic characteristics of a gradually accelerating aerofoil was developed at angles of attack as well as at zero angle of attack by conducting two-dimensional Navier-Stokes computations. To obtain different acceleration characters in a subsonic speed range, a non-dimensional acceleration factor was defined.

Computational results showed that an increase in the non-dimensional acceleration factor led to slower changes in the location and range of flow featues such as shockwave and boundary layer separation in a

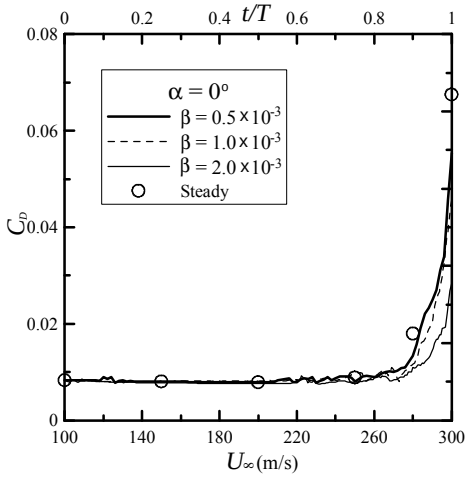

Fig. 7 Drag history during the acceleration at $\alpha = 0°$

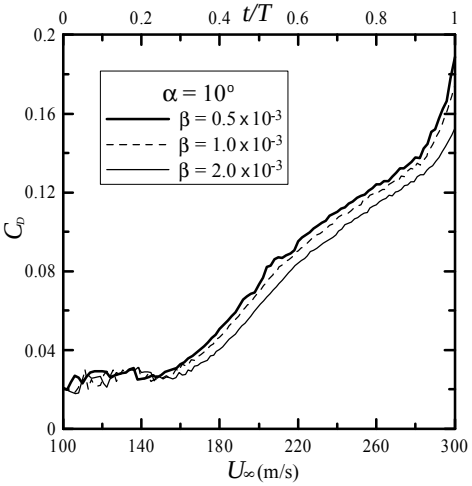

(a) Drag coefficient

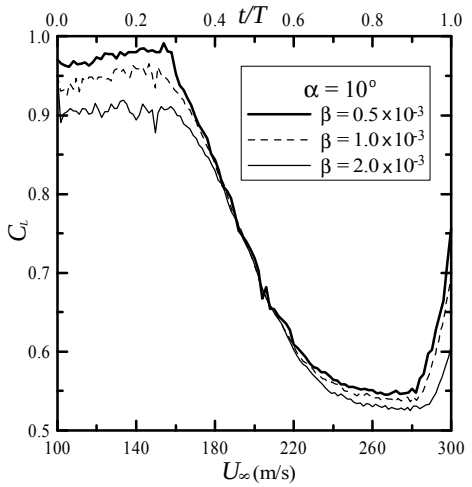

(b) Lift coefficient

Fig. 8 Drag and lift histories during the acceleration at $\alpha = 10°$

specific time range. The effect of the acceleration factor on aerodynamic characteristics was found to be more significant at angles of attack. Therefore, it was understood that flight stability at taking-off or at landing should be evaluated in consideration of particular aerodynamic characteristics for given accelerating time and speed range.

References

(1) Vos, J.B., Rizzi, A., Darracq, D. and Hirschel, E.H., 2002, "Navier–Stokes Solvers in European Aircraft Design," Prog. in Aerospace Sci., vol.24, pp.601-697.

(2) Kim, D.H. and Lee, I., 2000, "Transonic and Low-Supersonic Aeroelastic Analysis of a Two-Degree-of-Freedom Airfoil with a Freeplay Non-Linearity," J. Sound and Vibration, Vol.234, No.5, pp.859-880.

(3) Walsh, J.L., LaMarsh, W.J. and Adelman, H.M., 1993, "Fully integrated aerodynamic/dynamic optimization of helicopter rotor blades," Mathematical and Computer Modelling, Vol.18, Issues 3-4, pp.53-72.

(4) Ahmed, N., Yilbas, B.S. and Budair, M.O., 1998, "Computational Study into the Flow Field Developed around a Cascade of NACA 0012 Airfoils," Comput. Methods in Appl. Mech. and Engrg., Vol.167, pp.17-32.

(5) Akbari, M.H. and Price, S.J., 2003, "Simulation of Dynamic Stall for a NACA 0012 Airfoil Using a Vortex Method," J. Fluids and Structures, Vol.17, pp.855-874.

(6) Lee, B.H.K., 2001, "Self-sustained shock oscillations on airfoils at transonic speeds," Prog. in Aerospace Sci., Vol.37, pp.147-196.

(7) Mittal, S. and Saxena, P., 2002, "Hysteresis in Flow Past a NACA 0012 Airfoil," Comput. Methods in Appl. Mech. and Engrg., Vol.191, pp.2179-2189.

(8) Ericsson, L.E. and Reding, J.P., 1987, "Fluid Dynamic of Unsteady Separated Flow. Part II. Lifting surfaces," Prog. in Aerospace Sci., Vol.24, pp.249-356.

(9) Spalart, P.R. and Allmaras, S.R., 1992, "A One Equation Turbulence Model for Aerodynamic Flows," AIAA Paper 92-0439.

(10) Srinivasans, G.R., Ekaterinaris, J.A. and McCroskey, W.J., 1995, "Evaluation of Turbulence Models for Unsteady Flows of an Oscillating Airfoil," Computers & Fluids, Vol. 24, No. 7, pp.833-861.